Available online at www.sciencedirect.com
SCIENCE DIRECT®
PERGAMON
International Journal of Heat and Mass Transfer 46 (2003) 3299–3312
International Journal of HEAT and MASS TRANSFER
www.elsevier.com/locate/ijhmt

Validation of a model for the absorption process of H_2O(vap) by a LiBr(aq) in a horizontal tube bundle, using a multi-factorial analysis

Victor Manuel Soto Francés *, José Manuel Pinazo Ojer

Departamento de Termodinámica Aplicada, Universidad Politécnica de Valencia, Camino de Vera S/N, 456022 Valencia, Spain

Received 2 September 2002

Abstract

A multi-factorial experimental test of H_2O vapour absorption by a falling film of LiBr(aq) over an horizontal smooth tube absorber is presented. The response parameters of the study are the average convective heat transfer and mass transfer coefficients of the falling film. The response is expressed as a function of the factors used in the study. Also a mathematical model for the prediction of the performance of the absorber is exposed which takes into account the wetting effects. Finally the predictions from the model and the experimental multi-factorial runs are compared and the conclusions discussed.

Keywords: Absorption; Lithium bromide absorption machines; Absorber; Falling film; Modelling survey

1. Introduction

The development of absorption cooling machines goes through a deeper understanding of the physical and electrochemical processes involved. The processes should be viewed as a whole since electrochemical mechanisms are also important in practice, and affect all parts and processes inside the machine, including heat and mass transfer and liquid and solid phases (structural parts); as for instance, producing corrosion and H_2 (a non-condensable gas).

The heat and mass transfer processes occurring between the liquid and vapour phases are key points in sizing and designing the equipment.

The absorption process has been studied for several mixtures. The more common mixture pairs are; NH_3–H_2O and LiBr–H_2O. These studies are either theoretical or experimental, but only very few, like Wassenaar [2], have tried to compare the models with the experimental measurements. Killion and Garimella [1] did a comprehensive review on absorption with falling films and among their conclusions, we point out; (a) the experimental validation is very limited, (b) it is very difficult to compare the predictions, (c) the surface wetting is rarely incorporated. Therefore the applicability of the models to practical design is difficult, since it does not provide insight into the accuracy obtained by the hypothesis used in the model. The study has tried to overcome the aforementioned inconvenient aspects; (a)–(c).

The response parameters are usually a mass and a heat transfer coefficient defined in some way according to the driving forces selected. Unfortunately the behaviour of these response parameters are usually compared with seemingly, arbitrarily chosen parameters as for instance; non-dimensional parameters as the Reynolds' number, used by Lars [12], Miller [15] or Greiter et al. [16], and dimensional ones as the peripherical mass flow rate Γ, kinematic viscosity, surface tension, degree of subcooling, etc. (see [12,15]). However, it would be very interesting for the designer and researcher to have the

* Corresponding author. Tel.: +34-6-387-9326; fax: +34-6-387-7329.
E-mail address: vsoto@ter.upv.es (V.M. Soto Francés).

0017-9310/03/$ - see front matter
doi:10.1016/S0017-9310(03)00121-2

Nomenclature

Re	Reynolds number $4\Gamma/\mu$
Ga	Galileo number $\rho\sigma^3/\mu^4 g = Ka^{-1}$, $Ka \equiv$ Kapitza number
W	LiBr mass fraction [wt%]
μ	dynamical viscosity
D	Fick's diffusivity coefficient for the LiBr
P	pressure
X	wetted fraction
Δh_{abs}	enthalpy of absorption (enthalpy of the water vapour—partial enthalpy of water in the solution)

Greek symbols

Γ^+	non-dimensional peripherical mass flow rate
Γ	peripherical mass flow rate referred to one side of the tube [$kg\,s^{-1}\,m^{-1}$]
ρ	density
λ_0, λ	heat conductivity

Superscripts

$*$	equilibrium
–	average

Subscripts

cw	cooling water
i	inlet
o	outlet

information presented and treated in another way in order to be useful.

Devices for the experimental studies could be divided into small-scale experimental ones where the absorber geometry is not the one used in commercial machines, and medium size test rings which try to get closer to actual designs and working conditions. Examples of the first are; vertical or tilted plates and pools (the latter mainly for the study of the effects of additives).

In this work a medium size installation has been built. In the first part, a description is presented of the experimental test ring which tries to reproduce the most common commercial design; the falling film over a horizontal tube bundle.

In the second, it is presented shortly a mathematical model, for absorption of water vapour by aqueous LiBr solution for a whole absorber.

The experimental test has been organised in a multifactorial way, with a central test point. All those magnitudes, which were thought to be relevant and easy to change, were used as factors, and their effect studied afterwards by statistical analysis.

Smooth round copper tubes and LiBr(aq) solution without additive have been used to serve as a basis for checking the mathematical model and as a reference for future works.

2. Experimental set-up

The Fig. 1 shows a scheme of the installation. Basically its operation consists in generating water vapour, by heating a pool of aqueous LiBr solution with a variable salt concentration (54–61 wt% of salt, and a small amount of lithium chromate as corrosion inhibitor). The solution from the pool is pumped to the distribution tube at the top of the absorber and its temperature is adjusted to a value between the pool temperature and the outlet temperature of the cooling water. The solution falls over the horizontal tubes while absorbing the water vapour generated below. In order to maintain the absorption process, cooling water flows inside the tubes through the absorber almost countercurrently (with the inlet at the bottom tube). The measured magnitudes were the following:

At the absorber section:

- The water vapour pressure (capacitive sensor, P [see Fig. 1]).
- The temperature evolution of the cooling water. A differential temperature measurement was used between each pair of tubes (see [17,21]).

At the cooling water circuit:

- The cooling water temperature, at the inlet ($T_{cw,i}$) and outlet ($T_{cw,o}$) (Pt-100) and its volumetric flow rate (rotameter M3). The electrical heater D2 and the plate heat exchanger HX2 were used to adjust $T_{cw,i}$.

At the solution distribution circuit:

- Solution temperature at the inlet (T_i) and outlet (T_o) (Pt-100), and the solution mass flow rate (electromagnetic flow meter, M2). The plate heat exchanger HX3 and electrical heater D1 were used to adjust T_i.

At the concentration measurement circuit:

- Density and temperature of the solution, at the pool and the outlet of the absorber (Coriolis mass flowmeter, M1). These two magnitudes were used to estimate the salt mass fraction.

Auxiliary devices and circuits:

- The recirculation circuit was used for recirculating the solution in order to keep the pool concentration uniform during the tests. At the beginning of each test the valves of this circuit were used to measure

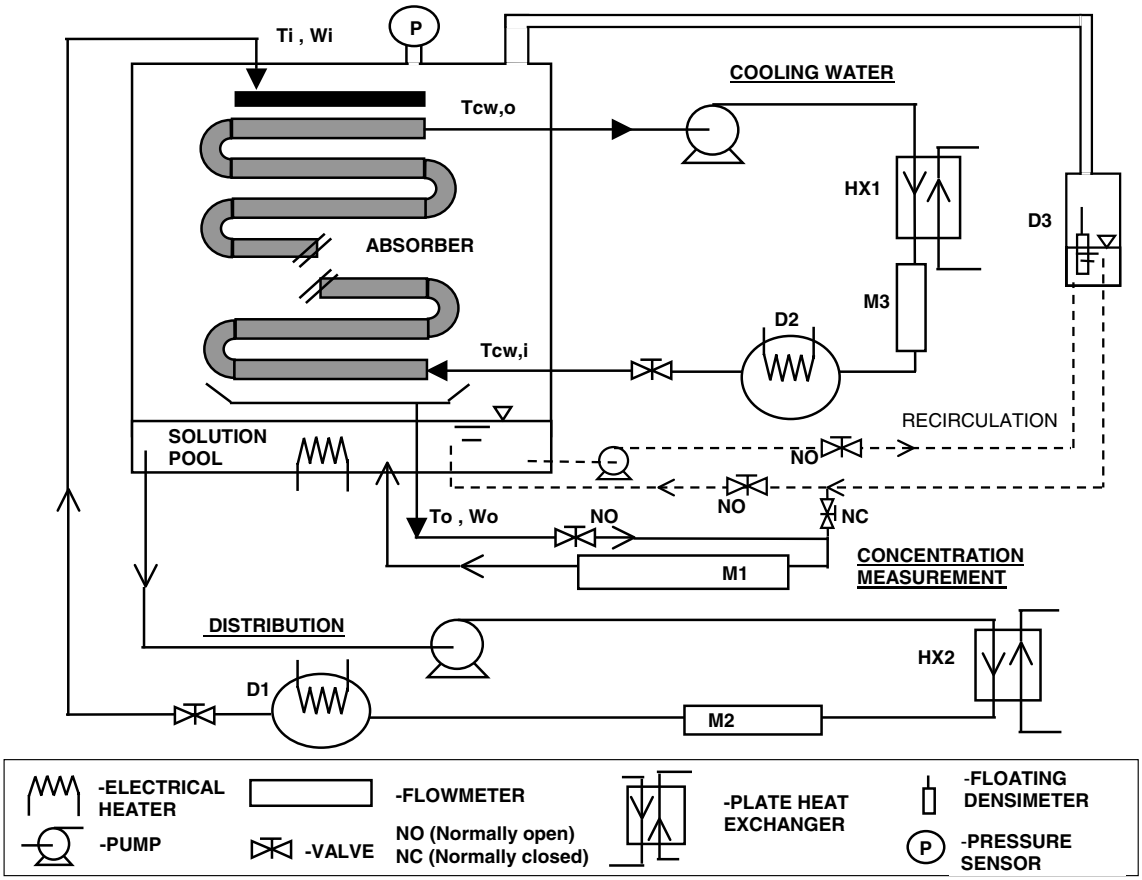

Fig. 1. Scheme of the installation; main circuits and components.

the pool concentration with the flowmeter M1. This circuit also had a floating densimeter D3 for checking visually the pool density.

The absorber was made up of 14 horizontal smooth copper tubes, 33 cm long. The external diameter was 15.9 mm and inside it was placed a concentric copper tube of 9.5 mm outer diameter to increase the cooling water side convective heat transfer coefficient. Through condensation experiences it was estimated to be 4039 $W\,m^{-2}\,°C^{-1}$.

The axes of the copper tubes were separated 46.9 mm, in order to achieve a higher mixing rate of the solution. The distributor tube at the top, had holes of a diameter of 1.5 mm and were separated 20 mm from each other. A static pressure head was maintained over each hole to assure a homogeneous distribution. The distance from the distributor to the first tube was 15 mm.

The copper tubes were electrically isolated with special connections and the same was done for other metals of the installation and the evolution of their electrical potential was recorded. The results allowed us to discover corrosion phenomena and also the production of H_2. Unfortunately, more research must be done at this respect.

3. Physical model for a tube

The bases of the physical model are those used already by other authors as Killion and Garimella [1], Wassenaar [2], Gierov and Jernqvist [18], Agunaoun et al. [19], Reisfeld and Bankoff [6], Choudhury et al. [20]. We resume them in what follows.

The mechanisms of heat and mass transport are; diffusion and convection in the radial direction. The hydrodynamics is supposed not to be influenced by these processes and therefore it is solved independently by neglecting density bulk effects and interfacial effects due to changes in surface tension (i.e. Marangoni convection).

The assumptions of the model are:

(1) The exchange is produced in stationary regime.
(2) The liquid is Newtonian. Its properties are calculated at the inlet of each tube and are kept constant for that tube.

(3) The flow is laminar and is described according to the Nusselt theory for completely developed flow. The mechanical force reactions of the vapour over the surface are also neglected.
(4) Exist thermodynamical equilibrium between the vapour and the solution at the interphase.
(5) All the heat is released at the surface and flows into the liquid film by conduction.
(6) The mixture is binary. The vapour contains only water.
(7) The diffusion of heat and mass is produced in radial direction.
(8) No crossed non-equilibrium effects such as; Soret o Dufour, are considered.
(9) Between tubes a complete mixing is assumed and therefore the concentration and temperature profiles at the top of each tube are uniform.

The 2D differential equations for heat and mass transfer, are the following:

$$u\frac{\partial T}{\partial x}+v\frac{\partial T}{\partial y}=\alpha\frac{\partial^2 T}{\partial y^2},\quad \alpha=\frac{\lambda_0}{\rho c_p} \tag{1a}$$

$$u\frac{\partial w}{\partial x}+v\frac{\partial w}{\partial y}=D\frac{\partial^2 w}{\partial x^2} \tag{1b}$$

and according to the hypothesis, the boundary conditions at the interphase are expressed as:

$$\Delta h_{\text{abs}}\frac{\rho D}{W}\left(\frac{\partial W}{\partial y}\right)\bigg|_{y=\delta}=-\lambda_0\left(\frac{\partial T}{\partial y}\right)\bigg|_{y=\delta} \tag{1c}$$

$$T|_{y=\delta}=f(P_{\text{vapour}},W_{y=\delta}) \tag{1d}$$

and at the tube wall:

$$-K_{\text{total}}(T|_{y=0}-T_{\text{cw}})=-K_{\text{total}}(T_{\text{wall,OD}}-T_{\text{cw}})=-\lambda_0\frac{\partial T}{\partial y}\bigg|_{y=0} \tag{1e}$$

$$\frac{\partial W}{\partial y}\bigg|_{y=0}=0 \tag{1f}$$

4. Discussion about the inter-tube flow

Hu and Jacobi [3,4] experimentally studied the hydrodynamics of the inter-tube flow. They used glycol with a sensible heat transfer and identified 6 modes; (I) droplets, (II) droplets-jets, (III) in-line jets, (IV) staggered jets, (V) jet-sheet and (VI) sheet. The transitions between modes are due to instabilities, which in turn are controlled by parameters of the flow.

Armbruster and Mitrovic [5] proposed a relationship for the parameters that control the inter-tube flow mode.

$$\left.\begin{aligned} Re&=\frac{2\Gamma}{\mu}\\ Ga&=\frac{\rho\sigma^3}{\mu^4 g}\end{aligned}\right\}\quad Re=aGa^{1/4} \tag{2}$$

From our observed working conditions, the inter-tube hydrodynamics belongs to the modes: (I) droplets or (II) droplets-jets/jets.

Using energetic considerations Hobbler [7], Hobbler and Czjka [8] first and Mikielewicz and Moszynski [9] afterwards, proposed a method for estimating the wetting fraction of a surface. Using their theory and after some algebra the following relationships for a plane surface, can be found:

$$Re=\Gamma^+\left(\frac{125}{9}\right)^{1/5}Ga^{1/5},\quad \Gamma^+=\left(\frac{9g}{125\rho\mu\sigma^3}\right)^{1/5}\Gamma \tag{3}$$

$$\Gamma^+_{\text{crit}}=\left(\frac{3}{2}\right)^{1/5}(1-\cos\theta_0)^{1/5} \tag{4}$$

where Γ^+ is a non-dimensional peripherical flow rate. Values lower than those obtained from Eq. (4), indicate that the tube is not completely wetted. Its critical value depends on the contact angle θ_0 as Eq. (4) shows. It is noteworthing that from the similarity between Eqs. (2) and (3), it might be inferred that the non-dimensional constant a in (2) should be proportional to Γ^+, thus giving to the constant a a physical meaning which was not realised by Jacobi and Hu. This can be corroborated looking at the empirical correlations for the mode transitions, which these authors gave in [3], and we reproduce here:

$$\begin{aligned} Re&=1.448Ga^{0.236}\quad(\text{sheet/jet-sheet})\\ Re&=1.414Ga^{0.233}\quad(\text{jet-sheet/jet})\\ Re&=0.096Ga^{0.301}\quad(\text{jet/jet-droplet})\\ Re&=0.074Ga^{0.302}\quad(\text{jet-droplet/droplet})\end{aligned} \tag{5}$$

The contact angle measured for LiBr over copper is $\theta_0=29.7°$ [10]. After substitution of Eq. (4) into Eq. (3) the critical Re obtained according to the wetting theory is:

$$Re=1.223Ga^{0.2} \tag{6}$$

To correct for round tubes instead of a plane, it suffices to modify the non-dimensional mass flow rate by a factor; $\Gamma^+_{\text{tube}}=1.1245\Gamma^+_{\text{plane}}$ [10], thus giving for the theoretical correlation:

$$Re=1.3752Ga^{0.2} \tag{7}$$

This expression is close to the sheet/jets-sheet correlation Eq. (5). Therefore according to our discussion, after the film rupture over the tube, the inter-tube flow changes; sheet → jets → droplets, with the non-dimensional flow rate Γ^+. As by visual observation the absorber always

Photo 1. On the left the inter-tube flow showing the jets/jets-droplets type of flow. An oscillating jet falls out of the absorber bundle. On the right the typical spatial wetting transition for the whole absorber is shown.

worked in modes (I) and (II), this means that there will always be a wetting problem (but for the case when a surfactant is added). This was corroborated experimentally (see Photo 1).

Finally from the theory it can be said that Γ^+ can also be used to estimate the steady wetted fraction after film rupture, as:

$$X = \frac{\Gamma^+}{\Gamma^+_{\text{critical}}} = \frac{\Gamma}{\Gamma_{\text{critical}}}, \quad \Gamma < \Gamma_{\text{critical}} \tag{8}$$

5. Wetting model for a whole tube bundle

The preceding discussion of Section 5, applies for a round tube under steady conditions and the flow fully developed spatially.

Nevertheless they are not valid for the whole absorber in practical conditions. The distributor over the first tube forces its complete wetting $X = 100\%$. In Photo 1 it can be seen the evolution of the wetting along the tube bundle. Wassenaar [2] observed also this evolution. The assumption of a completely wetted absorber leads to great prediction errors (see [17]), therefore taking the wetting into account is very important.

During the essays, at the beginning of the day, when all the installation was in thermal equilibrium, solution was pumped to the distributor onto the tube bundle. It was noticed that the pattern of the flow between the tubes was quiet inline-jets and the jets were fixed in space.

However when the cooling water started to flow and its temperature to decrease, thus leading to absorption conditions, the jets began to move laterally along the tube axis and oscillate in a plane perpendicular to the axis of the tube. The inter-tube flow changed into staggered jets or droplets-jets. This was more pronounced from the fourth row to the bottom, away from the distributor. It was possibly due to an uneven rate of water absorption on both sides of the tube thus producing surface tension unbalance. Eventually a jet fell outside the tube bundle as Photo 1 shows.

Our model does not take into account this phenomena and assumes that the mass flow rate is kept always flowing over the tubes. Also the kind of inter-tube flow and the conditions at the impinging zone are not considered.

Experimentally it was observed that from tube 10 to 14 the wetted fraction X were always the same for the four tubes. Its value was well predicted by Eq. (8). Therefore it was assumed that at this tube, fully developed wetting conditions were reached. The spatial transient evolution of the wetting from tube 1 ($X = 100\%$) at the top, to tube 10 and below, was adjusted as follows:

$$\begin{aligned} &\frac{X_j A}{2\pi d} = l_{\text{eff},j} = \mathrm{e}^{-\alpha(j-1)}, \quad j = 1,\ldots,10 \\ &\frac{X_j A}{2\pi d} = l_{\text{eff},j} = l_{\text{eff},10}, \quad j \geqslant 10 \end{aligned} \tag{9}$$

A is the area of a tube and α is an adjusting parameter. We used Eqs. (9) to define an effective length. The peripherical mass flow rate Γ must be recalculated for each tube according with this length l_{eff} (see [17]),

$$\Gamma_{j-1} l_{\text{eff},j-1} + \dot{M}_{\text{absorb}} = \Gamma_j l_{\text{eff},j} \tag{10}$$

In short, it can be said that the model takes into account Γ^+, regarding its wetting effect but not the inter-tube type of the flow and its corresponding impinging conditions.

6. Iteration through the absorber

Because the input or controlled data to the problem are the inlet conditions of the cooling water and of the solution, the computation of a whole absorber needs iteration. In our test section, the tube length was short enough to allow the hypothesis of a uniform average temperature for each tube, which in turn, is used to calculate an average heat and mass transfer for that tube. This can be expressed mathematically for tube j as:

$$(T^j_{\mathrm{cw,i}} + T^j_{\mathrm{cw,o}}) \cdot 0.5 = T^j_{\mathrm{cw}} \tag{11}$$

The computation procedure for the whole absorber is:

(1) Initial calculation of the conditions $\{(w^j_{\mathrm{LiBr}}, T^j)_{\mathrm{i}}, j = 2, \ldots, 14\}$, at the inlet of each j-tube assuming that $T^j_{\mathrm{cw}} = T^{14}_{\mathrm{cw,i}}$.
(2) For the evolution of the solution, this is the set $\{(w^j_{\mathrm{LiBr}}, T^j)_{\mathrm{i}}, j = 1, \ldots, 14\}$ fixed, the new set of cooling water temperatures at the outlet of each tube from tube 14 to 1 $\{T^j_{\mathrm{cw,o}}, j = 14, \ldots, 1\}$ is computed.
(3) In this (cooling water) iteration the heat exchanged by each tube is calculated, $\{Q^j_{\mathrm{cw}}, j = 14, \ldots, 1\}_{\mathrm{s}}$.
(4) For the next iteration a new average cooling water temperature evolution set $\{T^j_{\mathrm{cw}}, j = 1, \ldots, 14\}$ is computed with Eq. (11).
(5) With the average cooling water temperature set fixed, a new evolution of solution conditions is computed, $\{(w^j_{\mathrm{LiBr}}, T^j)_{\mathrm{i}}, j = 1, \ldots, 14\}$.
(6) In this solution side iteration, the heat exchanged by each tube is calculated, $\{Q^j_{\mathrm{cw}}, j = 1, \ldots, 14\}_a$.
(7) The pairs of iterations (3)–(4) and (5)–(6) continue until the following energy balance is fulfilled:

$$\sqrt{\sum_{j=1}^{N\ \mathrm{tubes}} (Q^j_{\mathrm{cw,s}} - Q^j_{\mathrm{cw,a}})^2} \leqslant \mathrm{tolerance} \tag{12}$$

7. Heat and mass transfer coefficients

In mass transfer problems, determination of the interfacial concentration is very important. However, in absorption plants is difficult to measure that concentration and for that reason it is very common that researchers define an average mass transfer coefficient using more accessible data. These data is taken normally at the inlet and outlet of the absorber for the lithium bromide solution.

Therefore for the average mass transfer coefficient (β), we used the following definition:

$$\beta = \frac{m_{\mathrm{absorbed}}}{A\rho\Delta W},$$
$$\Delta W = \frac{(W_{\mathrm{i}} - W^*_{\mathrm{i}}(P, T_{\mathrm{cw,o}})) - (W_{\mathrm{o}} - W^*_{\mathrm{o}}(P, T_{\mathrm{cw,i}}))}{\ln\left((W_{\mathrm{i}} - W^*_{\mathrm{i}}(P, T_{\mathrm{cw,o}}))/(W_{\mathrm{o}} - W^*_{\mathrm{o}}(P, T_{\mathrm{cw,i}}))\right)} \tag{13}$$

This definition is preferable to other used for example by Lars [11,12] or Miller [15] (see Eq. (14)).

$$\beta = \frac{m_{\mathrm{absorbed}}}{A\rho\Delta W},$$
$$\Delta W = \frac{(W_{\mathrm{i}} - W^*_{\mathrm{i}}(P, \overline{T}_{\mathrm{i}})) - (W_{\mathrm{o}} - W^*_{\mathrm{o}}(P, \overline{T}_{\mathrm{o}}))}{\ln\left((W_{\mathrm{i}} - W^*_{\mathrm{i}}(P, \overline{T}_{\mathrm{i}}))/(W_{\mathrm{o}} - W^*_{\mathrm{o}}(P, \overline{T}_{\mathrm{o}}))\right)} \tag{14}$$

The reason is that in case the mass transfer rate is such that the heat transferred to the cooling water is lower than the heat released by the absorption, it is possible for the solution temperature at the outlet to increase. This increase could lead, and in fact does for the case with additives, to an equilibrium salt concentration, at the vapour pressure, above the actual value at the outlet and therefore the logarithm would have a negative argument in Eq. (14). Although the mass transfer is an internal process, it is coupled in fact to the external conditions, for that reason we have employed Eq. (13) instead, which refers to the equilibrium concentration at the vapour pressure but at the cooling water temperature.

For the heat transfer the following expressions were used:

$$Q = AUF\Delta \ln T,$$
$$\Delta \ln T = \frac{(T_{\mathrm{i}} - T_{\mathrm{cw,o}}) - (T_{\mathrm{o}} - T_{\mathrm{cw,i}})}{\ln\left((T_{\mathrm{i}} - T_{\mathrm{cw,o}})/(T_{\mathrm{o}} - T_{\mathrm{cw,i}})\right)} \tag{15}$$

The absorber is treated as a counter-current heat exchanger. The corrective factor F is very close to unity (see [12]).The film heat transfer coefficient h_{film} is obtained from

$$\frac{1}{U} = \frac{r_{\mathrm{e}}}{h_{\mathrm{cw}} r_{\mathrm{i}}} + \frac{r_{\mathrm{e}} \ln(r_{\mathrm{e}}/r_{\mathrm{i}})}{\lambda_{\mathrm{copper}}} + \frac{1}{h_{\mathrm{film}}} \tag{16}$$

8. Multi-factorial test

It would be very interesting to give as many values as possible to all the factors but this would give us a huge number of runs.

For this reason, two levels have been chosen for each factor. Each level named as (L—low or H—high). The 5 factors and their ranges are shown in Table 1. This gives

Table 1
Factors used in the analysis and the values high and low given to them

A	W (wt%)	52–61%
B	$T_{\mathrm{cw,i}}$	30–35 °C
C	T_pool	40–46 °C
D	Γ	0.01–0.045 kg m^{-1} s^{-1}
E	V_{cw}	160–240 l h^{-1}

Table 2
Multi-factorial test

Run	W (wt% salt)		$T_{cw,i}$ (°C)		T_pool (°C)		Γ (kg m^{-1} s^{-1})		V_{cw} (l s^{-1})		Measured	
	Solution (A)		Cooling water (B)		Solution (C)		Solution (D)		Cooling water (E)		$\beta \times 10^5$ (m s^{-1})	h_{film} (W m^{-2} K^{-1})
1	L	52.43	H	36.25	L	40.44	L	0.0123	L	0.044	1.718	447
2	H	58.47	L	30.39	H	46.41	L	0.0126	L	0.044	0.399	704
3	L	52.42	L	30.83	H	46.46	H	0.0426	H	0.067	0.709	1239
4	H	57.94	H	35.33	H	46.37	L	0.0119	L	0.044	0.827	1091
5	L	52.71	L	30.98	L	40.03	H	0.0433	H	0.067	0.552	1231
6	H	57.94	H	35.33	H	46.36	H	0.0462	H	0.067	1.904	1320
7	H	57.94	H	36.31	L	41.31	H	0.0323	L	0.044	0.463	1307
8	H	57.94	H	35.94	L	40.26	L	0.0145	H	0.067	0.456	300
9	LH/2	55.61	LH/2	33.65	LH/2	43.44	LH/2	0.0287	LH/2	0.055	1.494	590
10	L	52.71	L	30.37	H	45.95	H	0.0371	L	0.044	1.502	1019
11	L	52.43	L	30.30	H	46.39	L	0.0103	H	0.067	2.700	741
12	H	58.47	L	30.63	H	46.44	H	0.0494	H	0.067	1.500	1051
13	L	52.71	L	30.58	H	46.01	L	0.0115	L	0.044	1.089	1089
14	H	58.47	L	30.73	H	46.43	L	0.0124	H	0.067	0.434	646
15	H	58.47	L	30.85	L	40.30	H	0.0464	H	0.067	0.727	1231
16	L	52.71	L	30.83	L	39.89	L	0.0266	H	0.067	0.451	483
17	L	52.71	H	36.26	L	40.40	H	0.0445	H	0.067	0.418	951
18	L	52.42	H	36.19	H	46.46	L	0.0123	L	0.044	1.268	614
19	H	58.22	L	30.48	L	41.23	L	0.0162	L	0.044	0.483	425
20	L	52.71	L	30.66	L	39.93	H	0.0457	L	0.044	0.598	1579
21	H	57.94	H	36.26	L	41.24	H	0.0479	H	0.067	0.777	1012
22	H	60.52	H	30.89	L	40.40	H	0.0149	H	0.067	0.303	517
23	L	52.71	L	30.39	L	39.60	L	0.0116	L	0.044	0.330	416
24	H	58.22	L	30.59	L	41.58	H	0.0462	L	0.044	1.281	1262
25	H	57.94	H	36.35	H	46.3	L	0.0145	H	0.067	1.114	620
26	L	52.42	H	36.53	H	46.46	H	0.0453	H	0.067	0.819	1181
27	H	60.79	L	30.49	H	46.48	H	0.0486	L	0.044	0.436	386
28	L	52.43	H	37.10	H	46.45	L	0.0104	H	0.067	4.150	438
29	L	52.42	H	36.29	H	46.48	H	0.0445	L	0.044	1.312	1047
30	L	52.61	H	35.83	L	40.45	L	0.0107	H	0.067	0.233	225
31	H	57.94	H	36.21	L	41.53	L	0.0150	L	0.044	0.518	442
32	L	52.61	H	36.02	L	40.39	H	0.0401	L	0.044	0.345	869
33	H	60.79	H	35.26	H	46.37	H	0.0481	L	0.044	1.731	1420

The table shows the numbers assigned to each run. The level of the factor for each run is also shown together with its actual average value obtained during the tests. On the right the table shows the measured average values of the film heat transfer coefficient h_{film} and the mass transfer coefficient β.

for the total number of combinations a value $2^5 = 32$ plus an extra central point. The central point has all the factors at a level in the middle of each range. Table 2 shows the number assigned to a run and its combination of factors.

The experimental heat transfer coefficient of the film h_{film} and the mass transfer coefficient β, have been correlated to a polynomial (named response surface) whose coefficients are shown in Appendix A. The resulting correlation explains the 72% for the dependency of both parameters on the factors.

Based on these polynomials, the direct influence of each factor on the transfer coefficients obtained from the experiences, together with their pair-wise interaction, can be analysed by the Pareto's Charts [21,23]. The Standardized Pareto's Charts have been also used to detect the influence of each experimental factor on the relative error between the measured and calculated values Eqs. (17a) and (17b). The x-axis is non-dimensional. It represents the standardized effect or in other words, the magnitude of the effect (change in the response) divided by its standard deviation for a certain factor. Statistically those factors whose bars are to the right of the vertical line must be considered the most important. The charts for the effect on the relative error in h_{film} and β, between the experience and the mathematical model, due to the chosen factors (see Table 1), are shown in Fig. 2. The discussion about the calculation of these errors and the results shown in Fig. 2, is found in the next section.

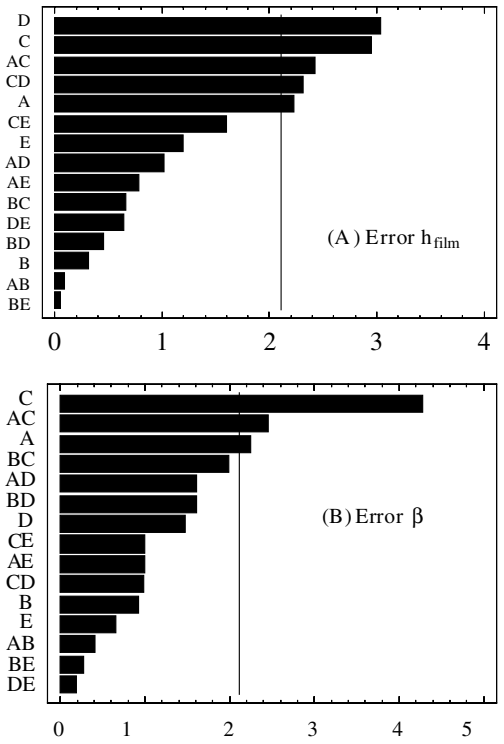

Fig. 2. Pareto's Charts for the analysis of the most influent factor and their binary interactions on the relative error between calculated and measured values (Eqs. (17a) and (17c) respectively): (A) h_{film} relative error and (B) β relative error. The x-axis is a non-dimensional scale for measuring the influence of each factor, it represents the value divided by its standard deviation.

9. Comparison experimental results vs. model results

The mathematical model provides data which is not accessible in the experiences as for instance, the interfacial concentration or the exact wetted fraction. Besides our purpose is to check if the hypothesis of the model are right. Therefore in order to be able to compare each other, we decided to lump the model as follows; the model was fed with the actual experimental inlet mean values corresponding to a certain run (see Table 2). After the calculations finished, its results at the inlet and outlet of the absorber were used to get the calculated average heat (h_{film}) and mass transfer (β) coefficient, and the total heat transferred (Q), in the same way as if the results had been produced experimentally. The relative errors between measured and calculated magnitudes are defined as:

$$h\,\text{relative error} = \frac{h_{\text{calculated}} - h_{\text{measured}}}{h_{\text{measured}}} \tag{17a}$$

$$Q\,\text{relative error} = \frac{Q_{\text{calculated}} - Q_{\text{measured}}}{Q_{\text{measured}}} \tag{17b}$$

$$\beta\,\text{relative error} = \frac{\beta_{\text{calculated}} - \beta_{\text{measured}}}{\beta_{\text{measured}}} \tag{17c}$$

In general the model predicts rather accurately the heat transfer coefficient and total heat Q exchanged (the mean absolute relative error $|h_{\text{film}_{\text{relative error}}}|$, is 22.4%). This value is slightly above the experimental error, 17%. Therefore it seems that the model can be used to predict the thermal load of the absorber (see Figs. 6 and 7).

It is worthwhile mentioning that the Reynolds' number variates a lot for a fixed Γ^+. That is due to the great variability of the viscosity with the salt concentration of the solution. Fig. 3 shows the dispersion plot for the runs used in our tests. Therefore, for the same Γ^+, which as was shown before, implies similar inter-tube hydrodynamic conditions and wetted fraction, very different Reynolds' numbers are possible and vice-versa.

From Figs. 4 and 5 the film heat transfer coefficient grows with Re while the mass transfer coefficient β grows from $Re = 0$ up to around $Re = 30$ and beyond decreases. Nevertheless, Fig. 4 shows a clearer correlation between h_{film} and Γ^+. Therefore the wetting of the tubes and the inter-tube flow controlled by this Γ^+, seem to be determinant factors for the heat transfer from the film to the tube, during absorption. We can deepen into this finding by comparing the results with the calculated values. The Pareto's chart for the error in the prediction of h_{film} (see Fig. 2), indicates that the most influent parameter on the deviation is the peripherical volume flow rate of solution Γ (factor D), followed by the T_pool and the interaction AC (T_pool and W). All of them could be lumped in Γ^+, since by fixing both, T_pool and W, the transport properties such as μ and ρ, σ, of the mixture are fixed. That means that some effect, due to Γ^+, is missed by the model. The explanation could be that our model lacks for the effect of the inter-tube type of flow. However as the predicted values are close to the mea-

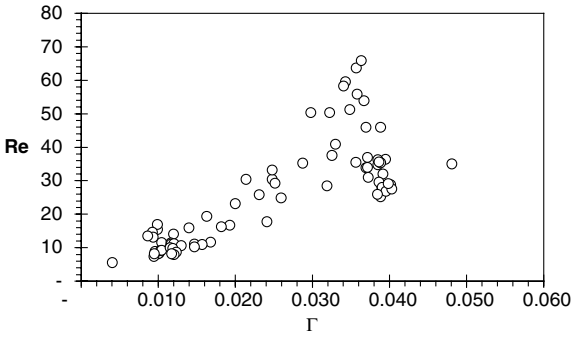

Fig. 3. Dispersion plot of the Reynolds' number with respect the non-dimensional peripherical flow rate Γ^+.

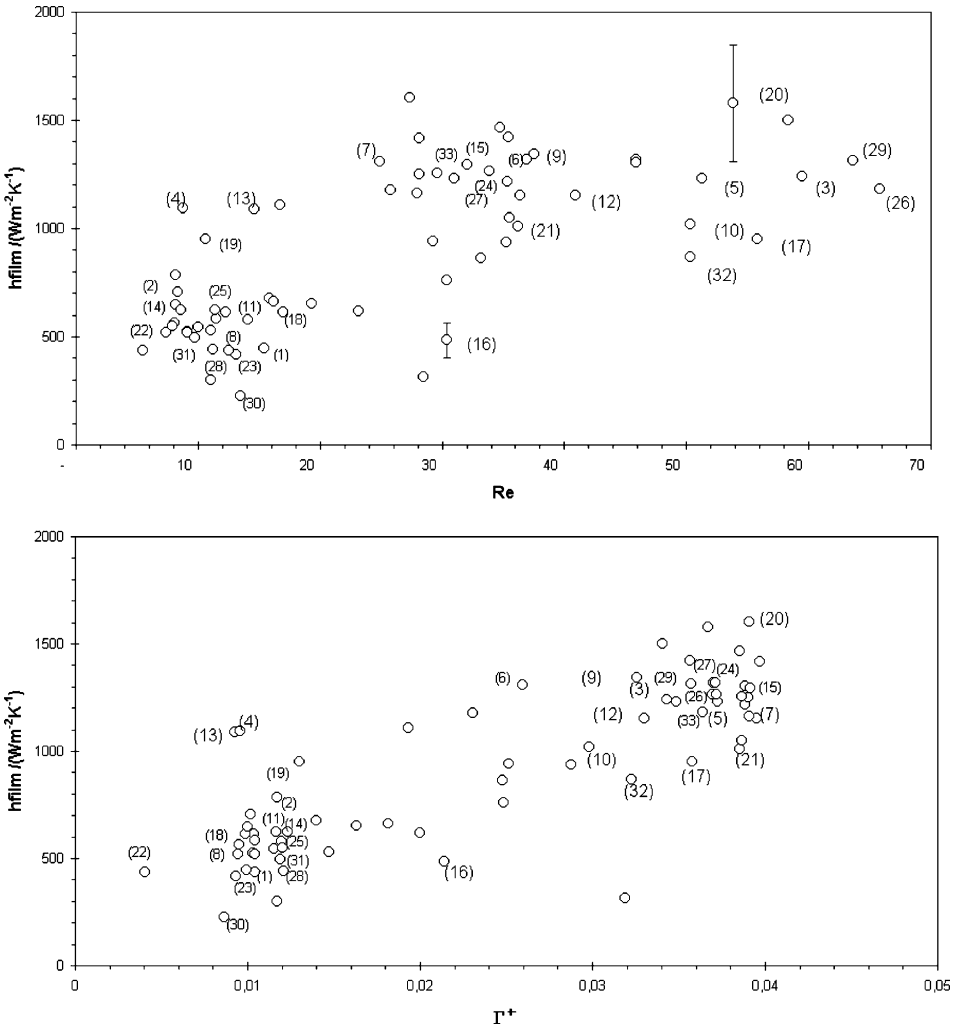

Fig. 4. Measured heat transfer coefficient of the film h_{film} ($\text{W m}^{-2}\,\text{K}^{-1}$) as a function of Re and Γ^{+}. The numbers in parentheses identify the runs of the multi-factorial test. The vertical bars indicate the order of accuracy of the measurements.

sured ones, it can be concluded that the inter-tube hydrodynamics has a much smaller effect than the more important one of the wetted fraction whose dependence on Γ^{+}, the model does consider (see [17]). This agrees with Wassenaar [2]. Nevertheless, it is noteworthy that the single effect of T_pool and even the concentration alone and their interaction (AC) are a source of error for the estimated value of h_{film}. This interaction is expressed by the following dependence found in the error; at high T_pool (46 °C) the influence of the concentration is small while at low T_pool (40 °C) its influence is high. In this last case, i.e. at lower temperatures, the error grows as the salt concentration decreases (52 wt% in our case). The same tendency is observed as well, for the mass transfer and it will be discussed below. In Fig. 6 it can be seen that the predictions, for the runs which fulfil the mentioned conditions, show the greater deviation.

Unfortunately, things are not so clear for the mass transfer coefficient β. The relative error of the prediction is high. The lower the actual value of β the higher its calculated value by the model (results are acceptable for $\beta > 1 \times 10^{-5}\ \text{ms}^{-1}$).

The mean absolute relative error $|\beta_{\text{relative error}}|$ is 119.34% while the experimental accuracy is 22%. Therefore the model is not good at predicting the mass transfer. The Fick's diffusivity coefficient employed in this work was measured by Gierow and Jerqvist [18] and agrees with other authors. When looking for another source of error one could think of the wetting or hydrodynamic aspects of the film. However after looking at the results, there are points with both high and low Γ^{+}, whose mass transfer is not well predicted. Moreover, this aspect does not seem to be crucial for the heat transfer predictions since they are quite good.

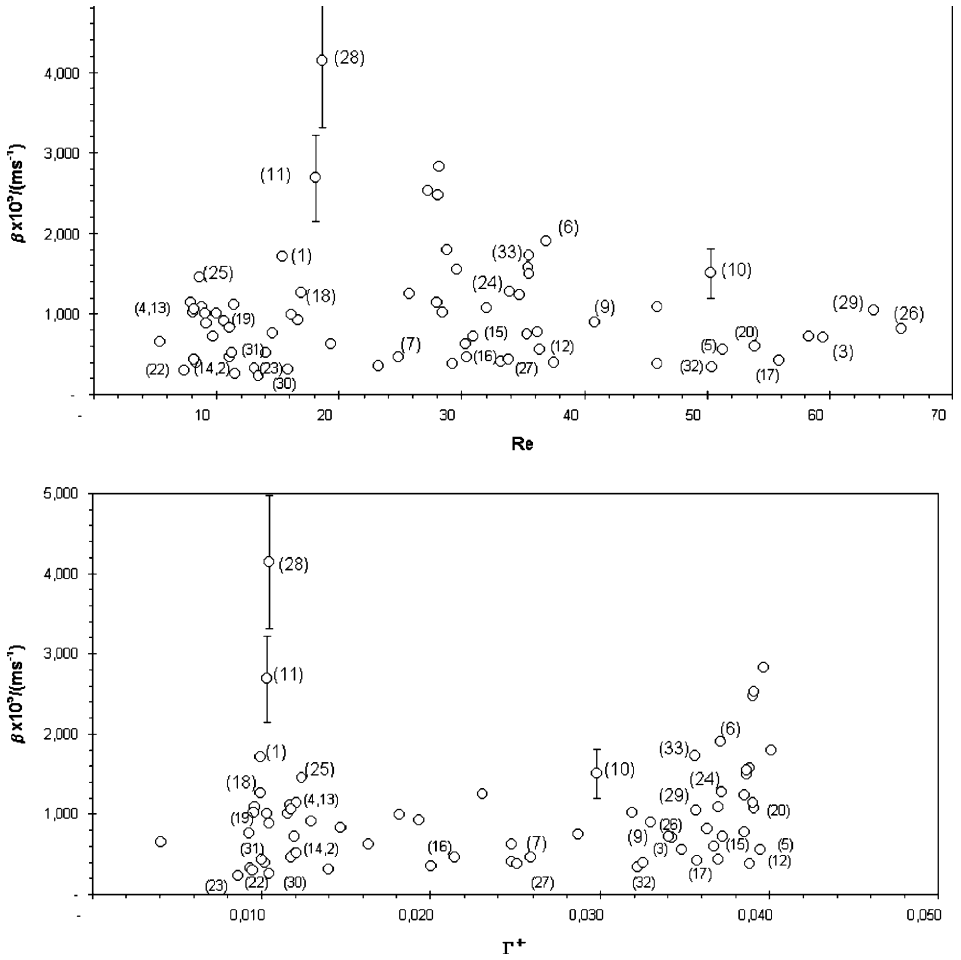

Fig. 5. Measured mass transfer coefficient $\beta \times 10^5$ ($m\,s^{-1}$) of the film as a function of Re and Γ^+. The numbers in parentheses identify the runs of the multi-factorial test. The vertical bars indicate the order of accuracy of the measurements.

The presence of non-condensable gases, which increase the mass transfer resistance, could be an explanation. At this respect it can be said that in the experiences, the installation was checked to vacuum down to a leakage below (10^{-3} mbar l s^{-1}). Moreover, previously to any day-run the installation was purged. The installation was able to keep the vacuum acceptably for a week. Besides those runs which show deviation, do not belong to the same day and some of them coincide in the same day, with runs that present a small error with respect to the prediction. For the runs, which produced a low coefficient of mass transfer, the film looked quiet while when conditions were changed producing a higher β the film swung perpendicular to the tube axis.

One more reason for the error could be that the model assumes a complete mixing between tubes. However if no mixing at all is assumed by keeping the concentration and temperature profiles from the bottom of one tube to the top of the next, not much better results are achieved.

In our opinion the marked overestimation in the prediction is intrigating, since it affects mainly the mass and not the heat transfer.

The analysis of the experimental results based on the calculated values with the Paretoás chart Fig. 2, indicates that the most influent factors in the error are; T_pool (C) followed by (AC) and W (A). The AC interaction is pointing to a dependence on the physical properties as before. Besides the dependence of the error on this interaction is just the same as for the h_{film}, commented above. From Fig. 5, if Γ^+ is used instead of Re as x-axis, a clearer separation of the runs appears but now their β values are spread wider than for h_{film}. Therefore it seems that the wetted fraction and perhaps the inter-tube flow, are not so determinant as for the heat transfer. This is also in agreement with

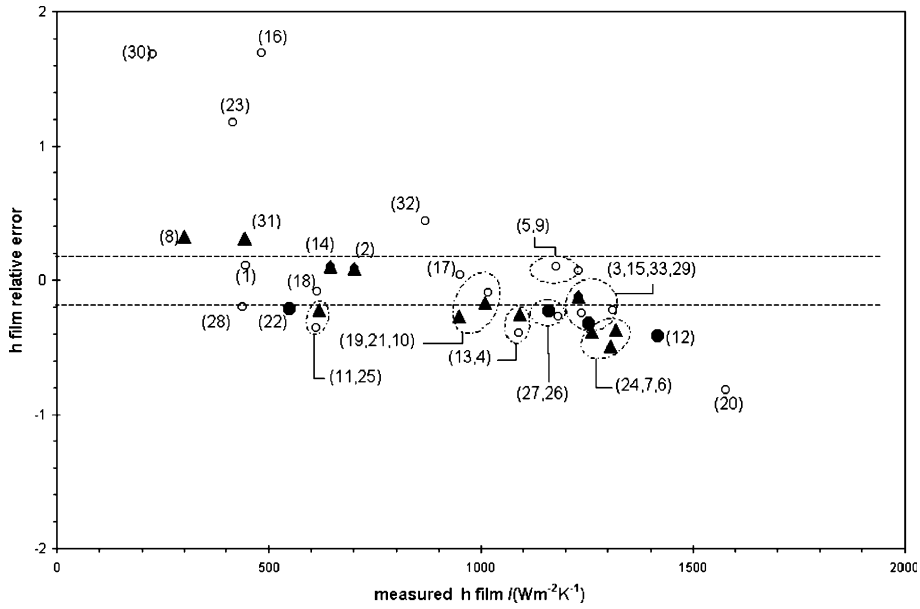

Fig. 6. Relative error between calculated and measured h_{film}. The two horizontal lines indicate the range of accuracy of the measurements. The numbers in parentheses identify the runs of the multi-factorial test: (○) $W = 52$ wt%, (▲) $W = 57.9$ wt%, (●) $W = 60.5$ wt%.

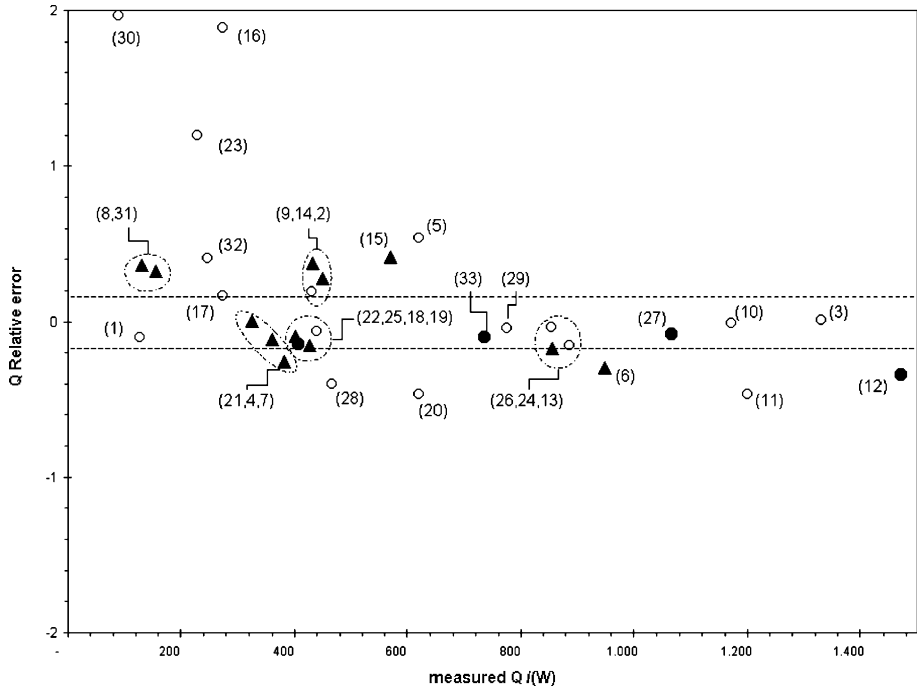

Fig. 7. Relative error between calculated and measured total heat exchanged Q (W) as a function of the measured value. The two horizontal lines indicate the range of accuracy of the measurement. The numbers in parentheses identify the runs of the multi-factorial test: (○) $W = 52$ wt%, (▲) $W = 57.9$ wt%, (●) $W = 60.5$ wt%.

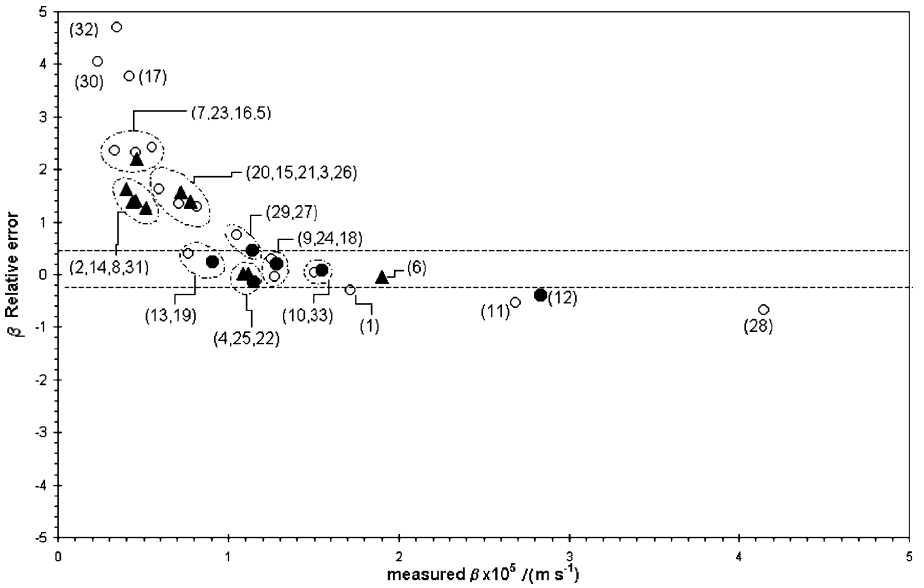

Fig. 8. Relative error between calculated and measured mass transfer coefficient $\beta \times 10^5$ ($m\,s^{-1}$). The numbers in parentheses identify the runs of the multi-factorial test. The two horizontal lines indicate the accuracy of the measurement: (○) $W = 52$ wt%, (▲) $W = 57.9$ wt%, (●) $W = 60.5$ wt%.

Wassenaar [2]. The single factor of the pool temperature, regardless of the value of any other factor, appears here once more as the leading factor. The fact that the error in the prediction is reduced when the salt concentration is high was not expected. Moreover, as Fig. 8 shows, the error is not always high for a certain concentration but depends on other factors, mainly on T_pool according to the analysis. At first sight it seems logical that the higher the W, the lower the pressure of the vapour and therefore it would have to be expected a greater sensibility of the mass transfer to the residual non-condensables gases. This would lead to an overprediction at higher concentrations, however the error shows just the opposite trend. Moreover the strong single effect of the T_pool independent of any other factor is rather strange. It must be pointed out that a higher T_pool also implies a higher T of the LiBr solution at the absorber inlet (distributor).

All this has led us to consider that perhaps a cross effect known as Soret effect (the mass diffusion due to thermal gradients) could be affecting the mass transfer (see Haase [14]). According to Colombani et al. [13] for the LiCl–H_2O, this effect is very strong (of the order $S_T = -10^{-3}$ K^{-1}) and for the LiBr–H_2O a similar effect is to be expected [22]. In LiCl(aq), S_T depends strongly on temperature and salt concentration. The form of this dependency agrees quite well with the results obtained for the error in the predicted β for mass transfer. The effect is stronger for the medium concentration range and decreases rapidly when salt concentration rises and weakens when the temperature rises.

Not only the value but the sign of the Soret S_T coefficient depends on the type of the electrolyte and also on the temperature and concentration. Unfortunately the reason for the sign is unknown since its microscopical mechanisms are still not clear. When $S_T < 0$ as for LiCl, the heavier component, the salt, goes towards the hotter places and it is likely to expect a similar behaviour also for LiBr. According to this, a hypothesis for explaining our results could be that the LiBr might move due to the temperature gradient, thus modifying in some way the liquid–vapour interphase and reducing its diffusive driving force into the bulk of the film, thus reducing the mass transfer. Unfortunately no complete data about the Soret effect for LiBr(aq) is available to our knowledge, and more research should be done.

10. Conclusions

The outcome of this work is to present the results of heat and mass transfer during absorption in a methodological way. A mathematical model whose main assumptions are widespread in the literature [1] has been used together with a wetting model. However the models of the literature are seldom compared with a range of experimental data generated systematically.

In this paper the multi-factorial study presented on h_{film} and β, gives a response surface as a function of the factors altered during the experiences, which has allowed

us to indicate a polynomial correlation f_o the study of the most influent factors and their binary interactions.

The model can be used to predict accurately the heat load and the average convective heat transfer coefficient of the film over the horizontal tube absorber. The h_{film} correlates well with Γ^+ which has been identified as the determinant parameter for the type of inter-tube flow and wetted fraction. It has been concluded also that the last one has more influence than the inter-tube type of flow, on the heat transfer in accordance with Wassenaar [2].

However the model is not good at predicting the mass transfer. The study shows that the single effect of the pool temperature and the concentration are the main factors affecting our predictions. It should be pointed out that both affect also the error in the prediction of the heat transfer and in the same manner, although the deviation is not so sharp.

We suspect that the hypothesis regarding mass transfer should be reviewed. Our opinion is that maybe the Soret effect at the surface, where the temperature gradients are high due to the sharp change of the physical properties, is playing some role. The study of its coupling with the heat and mass transfer processes should be studied and would be part of a future work.

Acknowledgements

We would like to thank the Spanish Government for their financial support through the project PB97-0336-C02-02, and to the UPV by its financial support through the "Plan de Innovación Tecnológica y Artística" no. 24.

Appendix A

h_{film} W m^{-2} °C^{-1}	
Constant	5062.0
$A : W_i$	−112.944
$B : T_{cw,i}$	−101.405
$C : P_{abs}$	−11.6975
$D : \Gamma$	−2779.87
E : cooling water flow	5.278
AB	2.94277
AC	−0.664776
AD	−100.111
AE	0.162705
BC	1.73227
BD	373.65
BE	−0.530034
CD	−86.9912
CE	0.0181368
DE	68.362

$\beta \times 10^5$ ms^{-1}	
Constant	−15.1205
$A : W_i$	0.18365
$B : T_{cw,i}$	0.534372
$C : P_{abs}$	0.0766905
$D : \Gamma$	71.2506
E : cooling water flow	−0.00236306
AB	−0.0057325
AC	−0.00192604
AD	0.581071
AE	−0.0000440625
BC	−0.00206042
BD	−3.74929
BE	−0.000096875
CD	1.07887
CE	0.000648437
DE	−0.00455357

$$Y = \text{constant} + a_A \cdot A + a_B \cdot B + \cdots + a_F \cdot F + a_{AB} \cdot A \cdot B + \cdots + a_{DE} \cdot D \cdot E$$

References

[1] D. Killion, S. Garimella, A critical review of coupled heat and mass transfer in falling-film absorption, Int. J. Refrig. 24 (2001) 755–797.
[2] R.H. Wassenaar, Measured and predicted effect of flowrate and tube spacing on horizontal tube absorber performance, Int. J. Refrig. 19 (5) (1996) 347–355.
[3] X. Hu, A.M. Jacobi, The intertube falling film: Part 1—Flow characteristics, mode transitions, and hysteresis, ASME Trans. 118 (1996) 616–625.
[4] X. Hu, A.M. Jacobi, The intertube falling film: Part 2—Mode effects on sensible heat transfer to a falling liquid film, ASME Trans. 118 (1996) 626–633.
[5] R. Armbruster, J. Mitrovic, Patterns of falling-film flow over horizontal smooth tubes, in: Proceedings of the Tenth International Heat Transfer Conference, vol. 3, 1994, pp. 275–280.
[6] B. Reisfeld, S.G. Bankoff, Non-isothermal flow of a liquid film on a horizontal cylinder, J. Fluid Mech. 236 (1992) 167–196.
[7] T. Hobler, Minimal Surface Wetting (en polaco), Chemia Stosow 2B 145 (1964).
[8] T. Hobler, J. Czjka, Doswiadczalme Sparwdzenie Teorii minimum Zraszania powierzchni, Chemia Stosow 2B 201 (1965).
[9] J. Mikielewicz, J.R. Moszynski, Minimum thickness of a liquid film flowing vertically down a solid surface, Int. J. Heat Mass Transfer 19 (1976) 771–776.
[10] J. Tang, B. Yu-Chi, Z. Lu, Minimum wetting rate of film flow on solid surface, in: Proceedings of the XVIIIth International Congress of Refrigeration, Montreal, vol. II, 1991, pp. 519–523.

[11] H. Lars, F. Ziegler, Heat and mass transfer enhacement by additives in NH_3–H_2O, in: ISHP'99 Proceedings of the International Sorption Heat Pump Conference, Munich.
[12] H. Lars, Bestimmung von Wärmeübergangskoeffizienten wässriger LiBr-Lösung mit und ohne Zusatz oberflächenaktiver Substanzen auf einem Absorberwärmetaucher, Diplomarbeit Institut E19 Physik-Department der Technischen Universität Muchen, 1994.
[13] J. Colombani, J. Bert, J. Dupuy-Philon, Thermal diffusion in LiCl, R-H_2O, J. Chem. Phys. 110 (17) (1999) 8622.
[14] Rolf Haase, Thermodynamics of Irreversible Processes, Dover Publications inc., New York, ISBN- 0-486-66356-6, 1969.
[15] W.A. Miller, The synergism between heat and mass transfer additive and advanced surfaces in aqueous LiBr horizontal tube absorbers, in: ISHPC'99, pp. 307–321.
[16] I. Greiter, A. Wagner, V. Weiss, G. Alefeld, Experimental investigation of heat and mass transfer in a horizontal-tube falling-film absorber with aqueous solutions, in: Proceedings of the International Absorption heat Pump Conference, ASME, 1994, pp. 225–232.
[17] V.M. Soto Francés, J.M. Pinazo Ojer, Experimental study about heat and mass transfer during absorption of water by an aqueous lithium bromide solution, in: Proceedings of the ASME-ZSITS International Thermal Science Seminar, Bled Slovenia, 11–14 June 2000.
[18] M. Gierow, A. Jernqvist, Measurement of mass diffusivity with holographic interferometry for H_2O/NaOH and H_2O/LiBr working pairs, in: Proceedings of the International Heat Pump Conference, AES, vol. 31, 1993, pp. 525–532.
[19] A. Agunaoun, A. Daïf, et al., Transfer de chaleur dans un film tombant autour d'un cylindre horizontal, Can. J. Chem. Eng. 72 (1994) 961–965.
[20] S.K. Choudhury, D. Hisajima, et al., Absorption of vapors into liquid films flowing over cooled horizontal tubes, ASHRAE Trans. 99 (2) (1993) 81–89.
[21] V. Soto Francés, Transferencia de Calor y Masa en absorbedores de tubos horizontales que trabajan con la mezcla LiBr-H_2O, Ph.D. Thesis, UPV Valencia 2000, ISBN: 84-699-4977-2.
[22] Colombani, private communication.
[23] Engineering Statistics Handbook. Available from: <http://www.itl.nist.gov/div898/handbook/pri/section5/pri597.htm>.